Inorg. Chem. **2005**, *44*, 2224–2233

Lead(II) Thiocyanate Complexes with Bibracchial Lariat Ethers: An X-ray and DFT Study

Carlos Platas-Iglesias, David Esteban-Gómez, Teresa Enríquez-Pérez, Fernando Avecilla, Andrés de Blas,* and Teresa Rodríguez-Blas*

Departamento de Química Fundamental, Universidade da Coruña, Campus da Zapateira, s/n, 15071 A Coruña, Spain

Received September 2, 2004

Compounds of formula [Pb(**L**^{2})(NCS)$_2$] (**1**) and [Pb(**L**^{4})(SCN)$_2$] (**2**) (where **L**^{2} is the lariat crown ether *N*,*N*′-bis(3-aminobenzyl)-4,13-diaza-18-crown-6 and **L**^{4} is the Schiff-base lariat crown ether *N*,*N*′-bis(3-(salicylaldimino)benzyl)-4,13-diaza-18-crown-6) were isolated and structurally characterized by X-ray diffraction analyses. The X-ray crystal structures of both compounds show the metal ion coordinated to the six donor atoms of the crown moiety, leaving the corresponding pendant arms uncoordinated. The coordination sphere of lead(II) is completed by two thiocyanate groups that coordinate either through their nitrogen (**1**) or sulfur (**2**) atoms. The organic receptor adopts a syn conformation in **1**, while in **2** it shows an anti conformation. To rationalize these unexpected different conformations of the **L**^{2} and **L**^{4} receptors in compounds **1** and **2**, as well as the different binding modes found for the thiocyanate ligands, we have carried out theoretical calculations at the DFT (B3LYP) level. These calculations predict the syn conformation being the most stable in both **1** and **2** complexes. So, the anti conformation found for **2** in the solid state is tentatively attributed to the presence of intermolecular π–π interactions between phenol rings, for which the dihedral angle between the least-squares planes of both rings amounts to 2.6° and the distance between the center of both rings is 3.766 Å. On the other hand, the analysis of the electronic structure has revealed that the Pb–ligand bonds present highly ionic character in this family of compounds. They also suggest a greater transfer of electron density from the NCS$^-$ ligands when they coordinate through the less electronegative S atom. The Pb–SCN covalent bond formation mainly occurs due to an effective overlap of the occupied 3p$_z$ orbitals of the S atoms and the unoccupied 6p$_z$ AO of the Pb atom, while the Pb–NCS bonding interaction is primarily due to the overlap of the 6s and 7s AO of Pb with sp$^{1.10}$ hybrids of the N donor atoms. Our electronic structure calculations can rationalize the different coordination of the thiocyanate groups in compounds **1** and **2**: the simultaneous formation of two Pb–SCN bonds is more favorable for S–Pb–S angles close to 180°, for which the overlap between the occupied 3p$_z$ orbitals of the S atoms and the unoccupied 6p$_z$ AO of the Pb atom is maximized.

Introduction

In general, transition metal complexes have common types of structures with specific coordination numbers, a fact that is strongly related to partly filled d orbitals of the central transition metal. Differently from transition metal complexes, non-transition-metal ones take various coordination numbers and in fact show diverse structures. The diversity of structures in non-transition-metal complexes is ascribed to the fact that d atomic orbitals of the metal center are fully occupied. However, non-transition-metal complexes have valence s and p electrons which can play an important role in determining their molecular structures. Transition metal complexes have been studied extensively both experimentally and theoretically, and many properties of transition metal complexes related to partly filled d orbitals of the metal ion are well explained in terms of ligand field theory.[1] However, relatively less theoretical studies on s and p block (non-transition) metal complexes have been reported to date.[2]

The chemistry of lead is of interest in relation to its toxicity and effects on intelligence in human populations.[3−5] The

* Authors to whom correspondence should be addressed. E-mail: mayter@udc.es (T.R.-B.).

(1) Schriver, D. F.; Atkins, P. W. *Inorganic Chemistry*, 3rd ed.; Oxford University Press: New York, 1999.
(2) Yamaki, T.; Nobusada, K. *J. Phys. Chem. A* **2003**, *107*, 2351.
(3) Hammond, P. B.; Foulkes, E. C. *Met. Ions Biol. Syst.* **1986**, *20*, 157.
(4) Goyer, R. A. In *Handbook on Toxicity of Inorganic Compounds*; Seiler, H. G., Sigel, H., Sigel, A., Eds.; Marcel Dekker: New York, 1988.
(5) Molin Christeensen, J.; Kristiansen J. In *Handbook on Metals in Clinical and Analytical Chemistry*; Marcel Dekker: New York, 1994.

10.1021/ic048768y CCC: $30.25
Published on Web 03/03/2005

Chart 1

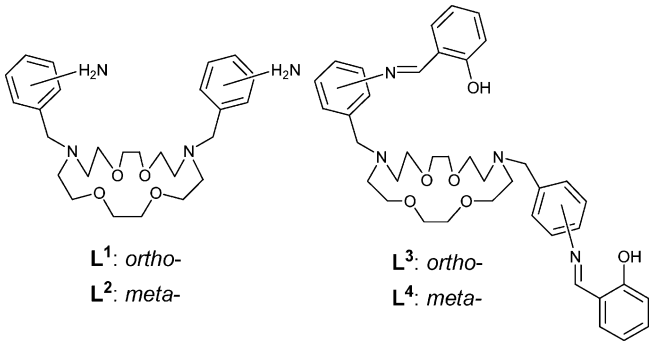

design of drugs to counteract the effects of lead poisoning requires establishing the preferred ligands of Pb(II) and their stereochemistry. This has caused a resurgence of interest in the coordination chemistry of Pb(II), and in recent years numerous reports concerning coordination chemistry of lead(II) with simple anions,[6] chelating ligands,[7] tripodal ligands,[8] and macrocycles[9] have been published. The lack of predictability associated with the coordination chemistry of lead(II) has been ascribed to the interplay of electrostatic factors and ligand constraints that might permit the stereochemical activity of the lead(II) lone pair to be expressed.[10] This factor is of considerable importance in attempts to design ligands which can be used in cases of lead intoxication, where selectivity is required for the large Pb(II) ion over the small Zn(II) ion.[11] To understand the experimental results, detailed electronic structure calculations of lead(II) complexes are needed.

Currently, we are interested in the coordination chemistry of lead(II) complexes supported by lariat crown ethers as shown in Chart 1.[12−14] In this study, we report the coordinating ability of the bibracchial lariat ethers $\mathbf{L^2}$ and $\mathbf{L^4}$ (Chart 1) toward the lead(II) ion, also in the presence of thiocyanate groups. The corresponding lead(II) complexes of formula [Pb($\mathbf{L^2}$)$(NCS)_2$] (**1**) and [Pb($\mathbf{L^4}$)$(SCN)_2$] (**2**) are characterized by X-ray diffraction analysis. To understand the structural features and electronic properties of these systems we turned to theory. Theoretical modeling has become an important tool to characterize coordination compounds. Density functional theory (DFT), especially the so-called hybrid HF-DFT functionals, has emerged as a very useful and cost-effective tool for investigating metal complexes. In the past few years, there have been a number of DFT studies of metal complexes with crown ethers[15,16] that were used to predict several properties such as molecular structure, relative stabilities, and NMR spectra. Compounds **1** and **2** are uncharged, which facilitate their study by theoretical methods. In particular, in this work we present a DFT study of these systems. The structures of the different isomers obtained from geometry optimizations were compared with the solid-state structures of **1** and **2**. Finally, a molecular orbital analysis of the metal−ligand bonds has been performed to get information about the chemical bond in this family of lead(II) compounds, as well as to rationalize the different coordination of the thiocyanate ligands in both complexes. We offer these results as proof that computational technology has now advanced to the point where predicted geometries and conformational energies of relatively complicated lead(II) complexes are in excellent agreement with the experimental findings.

Experimental Section

General Considerations. All chemicals were purchased from commercial sources and used without further purification. Solvents were of reagent grade purified by the usual methods. Elemental analyses were carried out on a Carlo Erba 1180 elemental analyzer. FAB mass spectra were recorded on a Fisons Quatro mass spectrometer with a Cs ion gun using 3-nitrobenzyl alcohol as matrix. ^{1}H and ^{13}C NMR spectra were run on Bruker AC 200F or Bruker WM-500 spectrometers. IR spectra were recorded, as KBr disks, using a Bruker Vector 22 spectrophotometer.

Syntheses and Characterization. Preparation of the Ligands. *N*,*N*′-Bis(3-nitrobenzyl)-4,13-diaza-18-crown-6. 4,13-Diaza-18-crown-6 (1.18 g, 4.50 mmol) and 3-nitrobenzyl chloride (1.54 g, 9.00 mmol) were dissolved in acetonitrile (60 mL), and solid Na_2CO_3 (2.4 g, 23.00 mmol) was added. The reaction mixture was stirred and refluxed for 24 h. After filtration, the filtrate was concentrated and the yellow oily residue was extracted with CH_2Cl_2/water. The organic phase was dried over anhydrous $MgSO_4$ and concentrated in vacuo, yielding a deep yellow solid (yield 2.08 g, 87%). Mp: 95 °C. Anal. Calcd for $C_{26}H_{36}N_4O_8$: C, 58.6; H, 6.8; N, 10.5. Found: C, 58.7; H, 6.9; N, 10.6. FAB-MS (*m*/*z* (% BPI)): 533 (100), $[M + H]^+$. IR (KBr): $\nu_{as}(NO_2)$ 1530, $\nu_s(NO_2)$ 1346 cm^{-1}. ^{1}H in CD_3CN: δ 8.25 (s, 2H, arH), 8.07 (m, 2H, arH), 7.79 (d, 2H, arH), 7.53 (t, 2H, arH), 3.81 (s, 4H, NCH_2ar), 3.60 (t, 8H, $-CH_2O-$), 3.56 (s, 8H, $-CH_2O-$), 2.77 (t, 8H, NCH_2-). ^{13}C in CD_3CN: δ 135.8, 130.1, 124.0, 122.5, 71.2, 70.4, 59.3, 54.8.

***N*,*N*′-Bis(3-aminobenzyl)-4,13-diaza-18-crown-6 Dihydrate ($\mathbf{L^2}$·2H_2O).** *N*,*N*′-Bis(3-nitrobenzyl)-4,13-diaza-18-crown-6 (1.06 g, 2.00 mmol) was dissolved in absolute ethanol (50 mL), and Pd/C was added. Hydrazine hydrate (82%, 7 mL) was slowly added, and the reaction mixture was heated and stirred for 4 h. It was then filtered, and the solvent was removed from the filtrate in a rotary evaporator. Addition of cold diethyl ether to the oily residue led to the deposition of a white precipitate (yield 0.70 g, 69%). Mp: 107 °C. Anal. Calcd for $C_{26}H_{40}N_4O_4$·2H_2O: C, 61.4; H, 8.7; N, 11.0. Found: C, 60.8; H, 8.6; N, 11.3. FAB-MS (*m*/*z* (% BPI)): 473 (100), $[\mathbf{L^2} + H]^+$. IR (KBr): $\nu_{as}(NH_2)$ 3450, $\nu_s(NH_2)$ 3305, $\delta(NH_2)$ 1626 cm^{-1}. ^{1}H in CD_3CN: δ 7.03 (t, 2H, arH), 6.67 (s, 2H, arH), 6.60 (d, 2H, arH), 6.53 (dd, 2H, arH), 3.55 (m, 12H, NCH_2ar, $-CH_2O-$), 3.58 (t, 8H, $-CH_2O-$), 2.73 (t, 8H, NCH_2-). ^{13}C in CD_3CN: δ 148.8, 130.5, 129.7, 118.8, 115.9, 113.9, 71.0, 70.0, 60.2, 54.7.

(6) Morsali, A.; Mahjoub, A. R. *Helv. Chim. Acta* **2004**, *87*, 2717.
(7) Fleischer, H.; Schollmeyer, D. *Inorg. Chem.* **2004**, *43*, 5529.
(8) Reger, D. L.; Wright, T. D.; Little, C. A.; Lamba, J. J. S.; Smith, M. D. *Inorg. Chem.* **2001**, *40*, 3810.
(9) Hancock, R. D.; Reibenspies, J. H.; Maumela, H. *Inorg. Chem.* **2004**, *43*, 2981.
(10) Parr, J. *Polyhedron* **1997**, *16*, 551.
(11) Hancock, R. D.; Shaikjee, M. S.; Dobson, S. M.; Boeyens, J. C. A. *Inorg. Chim. Acta* **1988**, *154*, 229.
(12) Esteban, D.; Bañobre, D.; de Blas, A.; Rodríguez-Blas, T.; Bastida, R.; Macías, A.; Rodríguez, A.; Fenton, D. E.; Adams, H.; Mahía, J. *Eur. J. Inorg. Chem.* **2000**, 1445.
(13) Esteban, D.; Avecilla, F.; Platas-Iglesias, C.; Mahía, J.; de Blas, A.; Rodríguez-Blas, T. *Inorg. Chem.* **2002**, *41*, 4337.
(14) Esteban, D.; Avecilla, F.; Platas-Iglesias, C.; de Blas, A.; Rodriguez-Blas, T. *Polyhedron* **2003**, *22*, 2709.
(15) Hambley, T. W.; Lindoy, L. F.; Reimers. J. R.; Turner, P.; Wei, G.; Widmer-Cooper, A. N. *J. Chem. Soc., Dalton Trans.* **2001**, 614.
(16) Platas-Iglesias, C.; Esteban, D.; Ojea, V.; Avecilla, F.; de Blas, A.; Rodríguez-Blas, T. *Inorg. Chem.* **2003**, *42*, 4299.

Preparation of the Lead(II) Complexes. Pb(L^2)$(SCN)_2$·H_2O (1). A solution of $Pb(SCN)_2$ (0.031 g, 0.097 mmol) in absolute ethanol (10 mL) was added to a stirred solution of the ligand **L²**·$2H_2O$ (0.046 g, 0.090 mmol) in absolute ethanol (10 mL). The reaction mixture was stirred under reflux for 17 h. During the course of the reaction, the solution became turbid and a white precipitate was deposited. This was collected by filtration, washed with diethyl ether, and air-dried (yield 0.045 g, 61%). Anal. Calcd for $C_{28}H_{40}N_6O_4PbS_2$·H_2O: C, 41.3; H, 5.2; N, 10.3. Found: C, 41.6; H, 4.8; N, 9.8. FAB-MS (*m*/*z* (% BPI)): 737, $[Pb(L^2)(SCN)]^+$; 679, $[Pb(L^1)]^+$. IR (KBr): $\nu_{as}(NH_2)$ 3424, $\nu_s(NH_2)$ 3338, $\delta(NH_2)$ 1623, (SCN) 2032 cm^{-1}. ^1H in CD_3CN: δ 7.12 (t, 2H, arH), 6.65 (d, 2H, arH), 6.58 (m, 4H, arH), 4.27 (br, 4H, $-NH_2$) 3.94 (br, 12H, NCH_2ar, $-CH_2O-$), 3.82 (b, 8H, $-CH_2O-$), 2.85 (b, 8H, NCH_2-). Slow diffusion of diethyl ether into a solution of **1** in acetonitrile gave single crystals of formula $[Pb(L^2)(NCS)_2]$ suitable for X-ray crystallography.

Pb(L^4)$(SCN)_2$·$1.5H_2O$ (2). *N*,*N*′-Bis(3-aminobenzyl)-4,13-diaza-18-crown-6 dihydrated (0.05 g, 0.11 mmol) and salicylaldehyde (0.03 g, 0.22 mmol) were dissolved in 2-propanol (60 mL), and the solution was heated to reflux. After 2 h $Pb(SCN)_2$ (0.05 g, 0.11 mmol) was added and the reflux was maintained for 2 h. The resultant deep yellow solution was filtered while hot and the filtrate rotary-evaporated to 20 mL. Upon cooling of the sample to room temperature, a yellow precipitate was formed and collected by filtration (yield 0.07 g, 63%). Anal. Calcd for $C_{42}H_{48}N_6O_6PbS_2$·$1.5H_2O$: C, 48.9; H, 4.9; N, 8.1. Found: C, 48.5; H, 4.6; N, 8.0. FAB-MS (*m*/*z* (% BPI)): 946, $[Pb(L^4)(SCN)]^+$; 887, $[Pb(L^4)]^+$. IR (KBr): $\nu(C{=}N)_{imine}$ 1618, SCN 2080 cm^{-1}. ^{13}C in $CDCl_3$: δ 163.5, 161.1, 148.7, 135.2, 134.3, 133.3, 132.6, 129.7, 129.3, 123.8, 119.2, 119.1, 117.2, 87.6, 69.6, 68.0, 52.0. Slow diffusion of diethyl ether into a solution of **2** in acetonitrile gave single crystals of formula $[Pb(\mathbf{L^4})(SCN)_2]$ suitable for X-ray crystallography.

Crystal Structure Determinations. Three-dimensional X-ray data for compounds **1** and **2** were collected on a Bruker Smart 1000 CCD operating at 20 °C. Data were corrected for Lorentz and polarization effects and for absorption by semiempirical methods. Both structures were refined by full-matrix least-squares on F^2. Complex scattering factors were taken from the program package SHELXTL.[17] Hydrogen atoms were included in calculated positions and refined in riding mode. The structure of **1** presents a disorder of one of the thiocyanate groups. This disorder has been resolved, and two atomic sites have been observed and refined with isotropic atomic displacement parameters for sulfur atom. The site occupancy factor for S(1SA) was 0.65(9). Crystal data and details on data collection and refinement are summarized in Table 1.

Computational Methods. The *syn*-[Pb(**L**)$(NCS)_2$] and *anti*-[Pb(**L**)$(SCN)_2$] systems (**L** = **L²** or **L⁴**, Scheme 1) were fully optimized by using B3LYP density functional model.[18,19] In these calculations we used the 3-21G* basis set for C and H atoms, while the 6-31G* basis set was used for N, O, and S atoms. For the Pb atoms, the LanL2DZ valence and effective core potential functions were used.[20,21] X-ray structures were used as input geometries when available. The stationary points found on the potential energy surfaces as a result of the geometry optimizations of **L²** complexes have been tested to represent energy minima rather than saddle points via frequency analysis. The complexes of **L⁴** were not characterized by frequency analysis due to the considerable effort required to calculate second derivatives in these systems. The relative free energies of the different isomers were calculated in vacuo at the same computational level, including nonpotential energy (NPE) contributions (that is, zero point energy and thermal terms) obtained by frequency analysis. The energy barrier and transition state for pendant arm rotation in the *syn*-[Pb(**L²**)$(NCS)_2$] and *anti*-[Pb(**L²**)$(SCN)_2$] systems were calculated in vacuo by means of the synchronous transit-guided quasi-Newton method.[22,23] The nature of the saddle points were characterized by frequency analysis. The wave functions of some of the lead complexes were analyzed by natural bond orbital analyses, involving natural atomic orbital (NAO) populations and natural bond orbitals (NBO).[24,25] All DFT calculations were performed by using the Gaussian 98 package (revision A.11.3).[26] Percentage compositions of molecular orbitals, overlap populations between molecular fragments, and density-of-states spectra were calculated using the AOMix program.[27,28] Density-of-states (DOS) and overlap population density-of-states (ODOS) plots were generated using Gaussian functions with half-widths of 0.1 eV.

Table 1. Crystal and Structure Refinement Data for **1** and **2**

	1	2
formula	$C_{28}H_{40}N_6O_4PbS_2$	$C_{42}H_{48}N_6O_6PbS_2$
M_r	795.97	1004.17
cryst system	monoclinic	monoclinic
space group	$P2_1/c$	$C2/c$
T/K	293(2)	293(2)
a/Å	19.4091(8)	27.180(3)
b/Å	8.9255(4)	10.6622(11)
c/Å	19.7706(8)	15.005(5)
β/deg	106.980(1)	96.234(2)
V/Å^3	3275.7(2)	4322.8(16)
F_{000}	1584	2016
Z	4	4
D_{calc}/g cm^{-3}	1.614	1.543
μ/mm^{-1}	5.319	4.052
R_{int}	0.1006	0.0492
reflcns measd	24 913	14 968
reflcns obsd	9396	5367
goodness-of-fit on F^2	0.917	0.902
R_1[a]	0.0542	0.0332
wR_2 (all data)[b]	0.1091	0.0839

[a] $R_1 = \Sigma||F_o| - |F_c||/\Sigma|F_o|$. [b] $wR_2 = \{\Sigma[w(|F_o|^2 - |F_c|^2|)^2]|/\Sigma[w(F_o^4)]\}^{1/2}$.

(17) Sheldrick, G. M. *SHELXTL*, release 5.1; Bruker Analytical X-ray Systems: Madison, WI, 1997.
(18) Becke, A. D. *J. Chem. Phys*. **1993**, *98*, 5648.
(19) Lee, C.; Yang, W.; Parr, R. G. *Phys. Rev. B* **1988**, *37*, 785.
(20) Hay, P. J.; Wadt, W. R. *J. Chem. Phys*. **1985**, *82*, 270.
(21) A description of the basis sets and theory level used in this work can be found in the following: Foresman, J. B.; Frisch, A. E. *Exploring Chemistry with Electronic Structure Methods*, 2nd ed.; Gaussian Inc.: Pittsburgh, PA, 1996.
(22) Peng, C.; Ayala, P. Y.; Schlegel, H. B.; Frisch, M. J. *J. Comput. Chem*. **1996**, *17*, 49.
(23) Peng, C.; Schlegel, H. B. *Isr. J. Chem*. **1994**, *33*, 449.
(24) Glendening, E. D.; Reed, A. E.; Carpenter, J. E.; Weinhold, F. *NBO*, version 3.1.
(25) Reed, A. E.; Curtiss, L. A.; Weinhold, F. *Chem. Rev*. **1988**, *88*, 899.
(26) Frisch, M. J.; Trucks, G. W.; Schlegel, H. B.; Scuseria, G. E.; Robb, M. A.; Cheeseman, J. R.; Zakrzewski, V. G.; Montgomery, J. A., Jr.; Stratmann, R. E.; Burant, J. C.; Dapprich, S.; Millam, J. M.; Daniels, A. D.; Kudin, K. N.; Strain, M. C.; Farkas, O.; Tomasi, J.; Barone, V.; Cossi, M.; Cammi, R.; Mennucci, B.; Pomelli, C.; Adamo, C.; Clifford, S.; Ochterski, J.; Petersson, G. A.; Ayala, P. Y.; Cui, Q.; Morokuma, K.; Malick, D. K.; Rabuck, A. D.; Raghavachari, K.; Foresman, J. B.; Cioslowski, J.; Ortiz, J. V.; Baboul, A. G.; Stefanov, B. B.; Liu, G.; Liashenko, A.; Piskorz, P.; Komaromi, I.; Gomperts, R.; Martin, R. L.; Fox, D. J.; Keith, T.; Al-Laham, M. A.; Peng, C. Y.; Nanayakkara, A.; Challacombe, M.; Gill, P. M. W.; Johnson, B.; Chen, W.; Wong, M. W.; Andres, J. L.; Gonzalez, C.; Head-Gordon, M.; Replogle, E. S.; Pople, J. A. *Gaussian 98*, revision A.11; Gaussian, Inc.: Pittsburgh, PA, 1998.
(27) Gorelsky. S. I. *AOMix program*, rev. 5.73; http://www.obbligato.com/software/aomix/.
(28) Gorelsky, S. I.; Lever, A. B. P. *J. Organomet. Chem*. **2001**, *635*, 187.

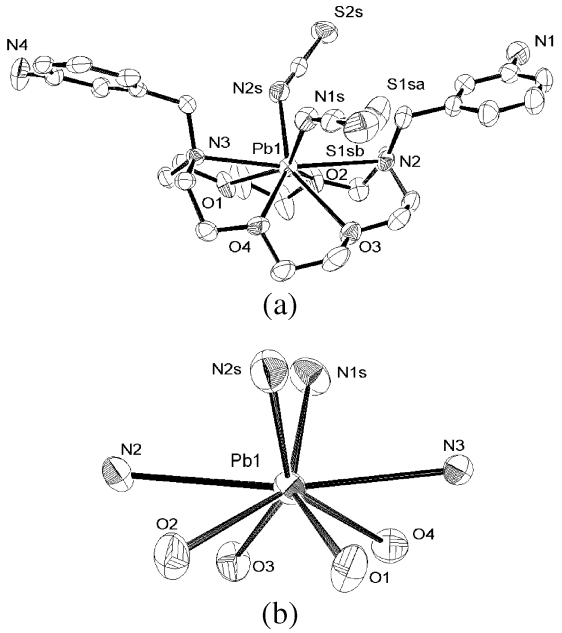

Figure 1. (a) X-ray crystal structure of **1**. Hydrogen atoms are omitted for simplicity. The structure presents a disorder of one of the thiocyanate groups, and two atomic sites (S(1SA) and S(1SB)) have been observed. The site occupancy factor for S(1SA) was 0.65(9). (b) View of the coordination polyhedron in **1**. The ORTEP plots are at the 30% probability level.

Results and Discussion

X-ray Crystal Structures of 1 and 2. Recrystallization of **1** from acetonitrile/diethyl ether gave colorless crystals suitable for single-crystal X-ray diffraction that contain the complex $[Pb(L^2)(NCS)_2]$. Figure 1 illustrates its structure, whereas bond lengths and angles of the coordination sphere are compiled in Table 2. Only six of the eight available donor atoms of $\mathbf{L^2}$ are coordinated to the lead(II) ion. Both aniline pendant arms remain uncoordinated. The lead(II) ion lies closer to one of the pivotal nitrogen atoms [Pb(1)−N(3) = 2.759(4) Å] than to the second one [Pb(1)−N(2) = 2.931(5) Å]. The latter distance is considerably longer than the sum of the van der Waals radius of nitrogen and the ionic radius of lead(II) (2.77 Å).[29,30] Eight-coordination is completed with two nitrogen atoms of the two isothiocyanate groups that coordinate from the same side of the crown moiety. The metal ion lies above the pseudoplane formed by the four oxygen atoms of the crown moiety. All the Pb−O distances fall within the range found for lead(II) complexes with similar crown receptors.[31]

The orientation of the aniline pendant arms of $\mathbf{L^2}$ can give rise to several conformational isomers that are illustrated in Figure 2. Both aniline pendant arms might be orientated on the same side of the macrocyclic plane, resulting in a syn conformation, or disposed in opposite sides of the crown moiety, giving rise to an anti conformation. Moreover, two conformations are possible for each syn and anti isomers depending on the relative orientation of the $-NH_2$ groups of both pendant arms. These two $-NH_2$ groups might be pointing to opposite sides of the crown moiety ((a) conformation) or to the same side ((b) conformations, Figure 2). In complex **1**, the macrocyclic receptor $\mathbf{L^2}$ adopts the so-called (b)-syn conformation in the solid state (Figure 1).

Table 2. Selected Bond Lengths (Å) and Angles (deg) for **1** and **2**

1		2	
Pb(1)−O(1)	2.713(4)	Pb(1)−O(3)	2.768(3)
Pb(1)−O(2)	2.753(4)	Pb(1)−O(2)	2.772(3)
Pb(1)−O(3)	2.824(4)	Pb(1)−N(2)	2.862(3)
Pb(1)−N(3)	2.759(4)	Pb(1)−S(1S)	2.9252(17)
Pb(1)−O(4)	2.801(4)		
Pb(1)−N(2S)	2.446(6)		
Pb(1)−N(1S)	2.504(6)		
Pb(1)−N(2)	2.931(5)		
N(2S)−Pb(1)−N(1S)	83.4(2)	O(3)−Pb(1)−O(2)	58.56(9)
N(2S)−Pb(1)−O(1)	78.99(19)	O(3)−Pb(1)−N(2)	60.90(9)
N(1S)−Pb(1)−O(1)	145.12(17)	O(2)−Pb(1)−N(2)	117.38(9)
N(2S)−Pb(1)−O(2)	75.68(18)	O(3)−Pb(1)−S(1S)	94.41(8)
N(1S)−Pb(1)−O(2)	142.54(18)	O(2)−Pb(1)−S(1S)	77.10(8)
O(1)−Pb(1)−O(2)	60.04(13)	N(2)−Pb(1)−S(1S)	93.19(8)
N(2S)−Pb(1)−N(3)	85.34(17)	O(3)−Pb(1)−S(1S′)	85.59(8)
N(1S)−Pb(1)−N(3)	84.66(17)	O(2)−Pb(1)−S(1S′)	102.90(8)
O(1)−Pb(1)−N(3)	64.20(13)	N(2)−Pb(1)−S(1S′)	86.81(8)
O(2)−Pb(1)−N(3)	123.39(14)	S(1S)−Pb(1)−S(1S′)	180.0
N(2S)−Pb(1)−O(4)	143.94(16)		
N(1S)−Pb(1)−O(4)	75.24(19)		
O(1)−Pb(1)−O(4)	102.50(14)		
O(2)−Pb(1)−O(4)	136.71(15)		
N(3)−Pb(1)−O(4)	64.27(13)		
N(2S)−Pb(1)−O(3)	146.71(18)		
N(1S)−Pb(1)−O(3)	83.03(17)		
O(1)−Pb(1)−O(3)	126.44(16)		
O(2)−Pb(1)−O(3)	97.68(15)		
N(3)−Pb(1)−O(3)	123.33(14)		
O(4)−Pb(1)−O(3)	59.09(13)		
N(2S)−Pb(1)−N(2)	87.50(18)		
N(1S)−Pb(1)−N(2)	86.85(17)		
O(1)−Pb(1)−N(2)	121.87(13)		
O(2)−Pb(1)−N(2)	61.83(14)		
N(3)−Pb(1)−N(2)	169.46(15)		
O(4)−Pb(1)−N(2)	119.34(14)		
O(3)−Pb(1)−N(2)	61.51(14)		

The coordination polyhedron around the metal in **1** may be described as a distorted trigonal prism that can be seen as comprised by two parallel tripods: N(1S), O(3), and O(4) form the upper tripod while N(2S), O(1), and O(2) delineate the lower tripod (Figure 1). The pivotal nitrogen atoms N(2) and N(3) are capping two of the three rectangular faces of the polyhedron. The mean twist angle of these two triangular faces (3.8°) is very close to the ideal value (0°) for a regular trigonal prism.[32] However, the angle between the planes defined by the upper and lower tripod amounts to 18.3°, showing a considerable distortion from the expected value for an ideal trigonal prism (0°).

The crystal packing in **1** is determined by intermolecular hydrogen-bonding interaction, which involves a proton of the amine group and a nitrogen atom of a isothiocyanate group of a neighboring molecule [N(4)···N(1S) 3.400 Å; N(4)H(4A)···N(1S) 2.62 Å; N(4)−H(4A)−N(1S) 150.7°]. Likewise, it could be stated that a weak intermolecular hydrogen-bonding interaction exists between a proton of the amine group and a sulfur atom of a isothiocyanate group of

(29) Aherens, L. H. *Geochim. Cosmochim. Acta* **1952**, *2*, 155.
(30) Pauling, L. *The Nature of the Chemical Bond*, 3rd ed.; Cornell University Press: Ithaca, NY, 1960.
(31) Byriel, K.; Dunster, K. R.; Gahan, L. R.; Kennard, C. H. L.; Latten, J. L.; Swann, I. L. *Polyhedron* **1992**, *11*, 1205.
(32) The mean twist angle between the two triangular faces of the trigonal prism is defined as in this paper: Elhabiri, M.; Scopelliti, R.; Bünzli, J.-C. G.; Piguet, C. *J. Am. Chem. Soc.* **1999**, *121*, 10747.

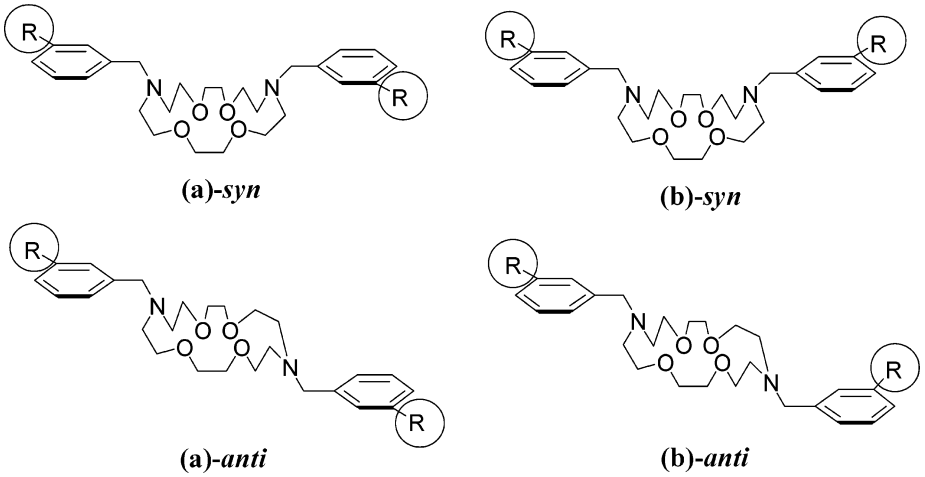

Figure 2. Schematic representation of the possible conformations of receptors $\mathbf{L^2}$ (R = $-NH_2$) and $\mathbf{L^4}$ (R = salicylaldimino) depending on the orientation of the aniline pendants.

a neighboring molecule [N(4)···S(2S) 3.712(8) Å; N(4)H(4B)···S(2S) 2.98 Å; N(4)−H(4B)−S(2S) 144.0°].

Recrystallization of **2** from acetonitrile/diethyl ether gave yellow crystals suitable for single-crystal X-ray diffraction that contain the complex [Pb($\mathbf{L^4}$)$(SCN)_2$]. Figure 3 illustrates its structure, whereas bond lengths and angles of the coordination sphere are compiled in Table 2. The molecule lies across a crystallographic inversion center, and the asymmetric unit contains a half-molecule. Again only the six available donor atoms of the crown moiety of the organic receptor are coordinated to the lead(II) ion, remaining both pendant arms uncoordinated. The phenol and imine groups of both pendant arms are involved in hydrogen-bonding interaction [O(1)···N(1) 2.627(6) Å; O(1)H(1)···N(1) 1.89 Å; O(1)−H(1)−N(1) 148.2°].

In contrast to the observed for **1**, in **2** the lead(II) ion fits inside the crown hole and both pendant arms are arranged on opposite sides with respect to the crown moiety. Both imine groups are also oriented to opposite sides of the crown moiety, and the conformation of receptor $\mathbf{L^4}$ in **2** is described as (a)-anti (Figures 2 and 3). Eight-coordination is completed with two sulfur atoms of the two thiocyanate groups that coordinate from opposite sides of the crown moiety. The coordination polyhedron in **2** may be described as a distorted hexagonal bipyramid (Figure 3b) in which atoms O(3), O(2), N(2), O(3′), O(2′), and N(2′) form the equatorial plane (mean deviation from planarity 0.2341 Å) and atoms S(1S) and S(1S′) occupy the axial positions. Angles S(1S′)−Pb(1)−O(3) [85.59(8)°], S(1S′)−Pb(1)−O(2) [102.90(8)°], and S(1S)−Pb(1)−N(2) [93.19(8)°] are close to the ideal values for a hexagonal bipyramid (90°). Angles O(3)−Pb(1)−O(2) [58.56(9)°] and O(3)−Pb(1)−N(2) [60.90(9)°] are also close to the expected values (60°). Moreover, the S(1S)−Pb(1)−S(1S′) angle amounts to 180°, as expected for a regular hexagonal bipyramid.

The crystal packing in **2** is determined by intermolecular interactions between the phenol aromatic rings. These aromatic rings are nearly parallel, with a dihedral angle between the least-squares planes of both rings amounting to 2.6°. Moreover, the distance between the center of both rings is 3.766 Å, so that intermolecular $\pi-\pi$ interactions are possible.[33,34]

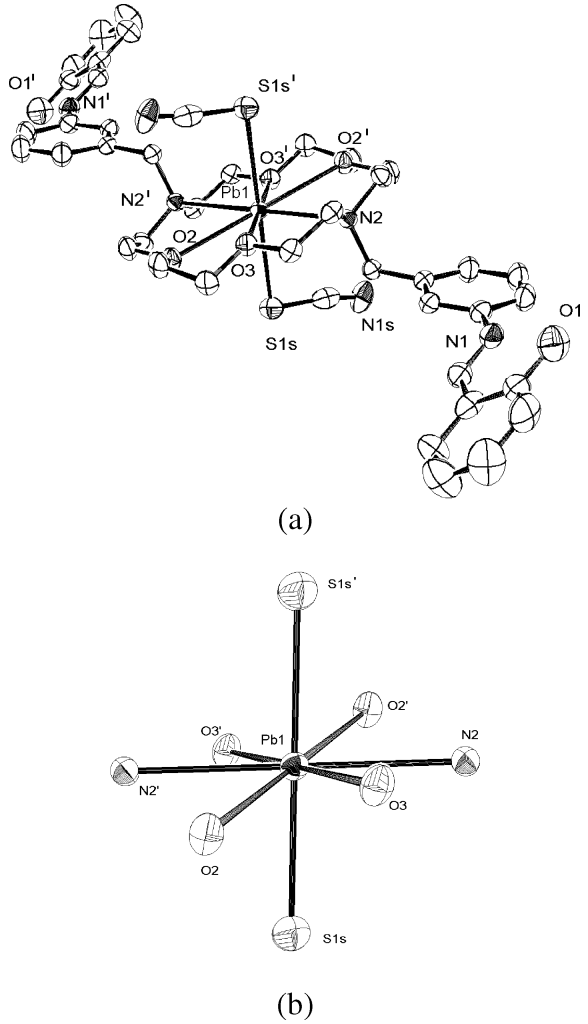

Figure 3. (a) X-ray crystal structure of **2**. Hydrogen atoms are omitted for simplicity. (b) View of the coordination polyhedron in **2**. The ORTEP plots are at the 30% probability level.

(33) Ranganathan, D.; Haridas, V.; Gilardi, R.; Karle, I. L. *J. Am. Chem. Soc*. **1998**, *120*, 10793.
(34) Lahiri, S.; Thompson, J. L.; Moore, J. S. *J. Am. Chem. Soc*. **2000**, *122*, 11315.

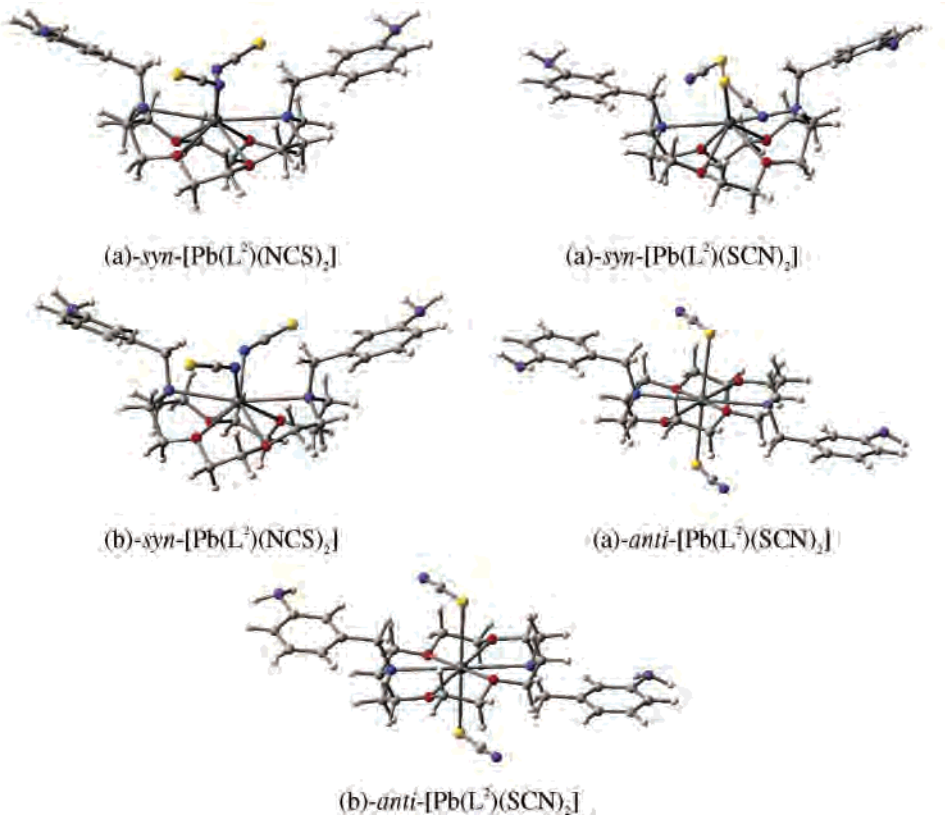

Figure 4. Structure of syn and anti isomers of lead(II) complexes of $\mathbf{L^2}$ as optimized in vacuo at the B3LYP level.

Geometry Optimizations. Aiming to understand the reasons for the different conformations observed in the solid state for compounds **1** and **2**, we have carried out a conformational investigation of the Pb(II) thiocyanate complexes of $\mathbf{L^2}$ and $\mathbf{L^4}$ by means of DFT calculations (B3LYP model). In these calculations we used the 3-21G* basis set for C and H atoms, while the 6-31G* basis set was used for N, O, and S atoms. As there is not any all-electron basis set for lead, the effective core potential of Wadt and Hay (Los Alamos ECP) included in the LanL2DZ basis set was applied in these calculations.[20,21] Compared to all-electron basis set, ECPs account for relativistic effects to some extent. It is believed that relativistic effects will become important for the elements from the fourth row of the periodic table.[35] This ECP has been demonstrated to provide reliable results for different Pb(II) coordination compounds.[2,36−38] For the $\mathbf{L^2}$ complexes the four possible conformations shown in Figure 2 were explored. The lowest energy geometries located for the complexes of $\mathbf{L^2}$, which were found to correspond to minima in the potential energy surface, are shown in Figure 4. Due to the important computational effort required to perform geometry optimizations for the complexes of $\mathbf{L^4}$ only the (b)-*syn*-[Pb(L^4)$(NCS)_2$] (**1**) and (a)-*anti*-[Pb(L^4)$(SCN)_2$] conformations were explored, since they correspond to the minimum energy conformations calculated for the corresponding complexes of $\mathbf{L^2}$. The minimum energy geometries calculated for these complexes of $\mathbf{L^4}$ are shown in Figure 5.

The solid-state X-ray crystal structures of compounds **1** and **2** described above are quite similar to the in vacuo optimized structures of (b)-*syn*-[Pb(L^2)$(NCS)_2$] and (a)-*anti*-[Pb(L^4)$(SCN)_2$]. Both calculated structures show bond distances of the Pb coordination sphere in reasonable agreement with the experimental ones (Table 3). The calculated structures of (a)- and (b)-isomers indicate that the rotation of one of the pendant arms does not induce important changes in the Pb(II) coordination environment (Table 3). For a given conformation (syn or anti) the calculated Pb−donor bond distances are very similar in both $\mathbf{L^2}$ and $\mathbf{L^4}$ complexes, indicating that the introduction of two salicylaldimino subtituents in the pendant arms of $\mathbf{L^2}$ does not significantly modify the coordinative properties of the macrocyclic receptor. The in vacuo optimized Cartesian coordinates obtained for the different systems studied in this paper are given in the Supporting Information.

Conformational and Strain Energies. The relative free energies of calculated syn and anti configurations for the lead(II) complexes of $\mathbf{L^2}$ and $\mathbf{L^4}$ are listed in Table 3. In parallel to the results from the X-ray studies, the syn configurations of $\mathbf{L^2}$ complexes were found by DFT to be those of lowest energy by ca. 50 kJ mol^{-1}. The calculated minumum energy conformation corresponds to the (b)-*syn*-[Pb(L^2)$(NCS)_2$] structure, in agreement with the X-ray data. Our DFT calculations also predict the (b)-*syn*-[Pb(L^4)$(NCS)_2$] structure being more stable than the (a)-*anti*-[Pb(L^4)$(SCN)_2$]

(35) Harrington, J. M.; Jones, S. B.; White, P. H.; Hancock, R. D. *Inorg. Chem.* **2004**, *43*, 4456.
(36) Shimoni-Livny, L.; Glusker, J. P.; Bock, C. W. *Inorg. Chem.* **1998**, *37*, 1853.
(37) Di Vaira, M.; Mani, F.; Constantini, S. S.; Stoppioni, P.; Vacca, A. *Eur. J. Inorg. Chem.* **2003**, 3185.
(38) Akibo-Betts, G.; Barran, P. E.; Puskar, L.; Duncombe, B.; Cox, H.; Stace, A. J. *J. Am. Chem. Soc.* **2002**, *124*, 9257.

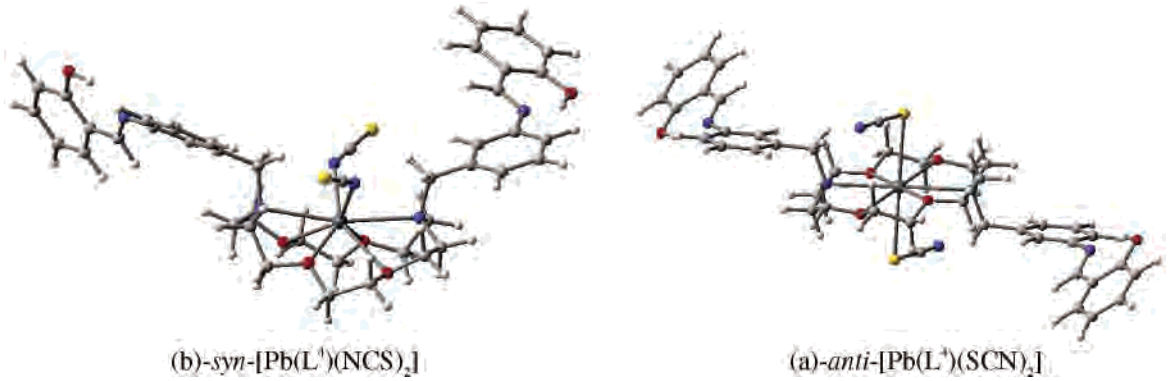

Figure 5. Structure of syn and anti isomers of lead(II) complexes of $\mathbf{L^4}$ as optimized in vacuo at the B3LYP level.

Table 3. Mean Distances (Å) of Experimental and Calculated Structures,[a] in Vacuo Relative Free Energies ($\Delta G°_{298K}$, kJ mol^{-1}), and Relative Strain Energies (kJ mol^{-1}) of Pb(II) Complexes of $\mathbf{L^2}$ and $\mathbf{L^4}$ Obtained from DFT Calculations

compd		Pb−O	Pb−N[b]	Pb−N[c]	Pb−S	$\Delta G°_{298K}$[d]	strain energy[e]
(a)-*syn*-[Pb($\mathbf{L^2}$)(NCS)$_2$]	calcd	2.82(7)	2.826(3)	2.391(0)		4.0	0.3
(a)-*syn*-[Pb($\mathbf{L^2}$)(SCN)$_2$]	calcd	2.79(7)	2.877(0)		2.927(0)	56.5	13.2
(b)-*syn*-[Pb($\mathbf{L^2}$)(NCS)$_2$]	calcd	2.82(7)	2.826(6)	2.385(5)		0.0	0.0
	X-ray	2.77(6)	2.85 (9)	2.48(3)			
(a)-*anti*-[Pb($\mathbf{L^2}$)(SCN)$_2$]	calcd	2.80(4)	2.90(1)		2.99(3)	53.7	7.9
(b)-*anti*-[Pb($\mathbf{L^2}$)(SCN)$_2$]	calcd	2.80(1)	2.904(4)		2.989(1)	53.9	9.7
(b)-*syn*-[Pb($\mathbf{L^4}$)(NCS)$_2$]	calcd	2.83(7)	2.82(1)	2.389(8)		0.0	0.0
(a)-*anti*-[Pb($\mathbf{L^4}$)(SCN)$_2$]	calcd	2.80(2)	2.911(3)		2.990(0)	46.5	7.5
	X-ray	2.770(2)	2.862		2.9252		

[a] The average values are reported with standard deviations in parentheses. [b] Tertiary amine. [c] Isothiocyanate nitrogen. [d] In vacuo relative free energies include corrections for NPE terms for the complexes of $\mathbf{L^2}$. [e] The strain energies (of the macrocyclic ligands) are the relative energies of the ligands in their geometry found within the complexes.

one, in contrast with the X-ray evidence (Table 3). However, this is not surprising since ligands $\mathbf{L^2}$ and $\mathbf{L^4}$ are expected to have similar donor capabilities toward lead(II) because their pendant arms remain uncoordinated in the corresponding complexes. The *anti*-[Pb(L^4)(SCN)$_2$] configuration observed in the solid state can be tentatively attributed to a more favorable crystal packing for this conformation due to the presence of intermolecular $\pi-\pi$ interactions between phenol rings (vide supra).

The greater stability of the syn complexes in both $\mathbf{L^2}$ and $\mathbf{L^4}$ complexes appears to reflect a reduction in strain of the coordinated ligand (Table 3). The relative free energies of (a)- and (b)-conformations of $\mathbf{L^2}$ complexes within a given syn or anti geometry are small, and they amount to 4.0 (syn) and 0.2 (anti) kJ mol^{-1}. These small values are a consequence of the negligible effect that the rotation of the pendant arm has on the ligand strain energy (Table 3).

Pb(II) is classified as "intermediate" in the Pearson HSAB classification,[39] and thus it is not particulary surprising the existence of both N-bonded and S-bonded Pb(II) complexes of thiocyanate. It has been suggested that steric hindrance around the metal ion favor the coordination of the SCN$^-$ ligands through the N donor atom.[40] To investigate whether steric effects are responsible for the different binding mode of the thiocyanate ligands in **1** and **2** we performed geometry optimizations on the (a)-*syn*-[Pb(L^2)(SCN)$_2$] system, where the SCN$^-$ groups are S-bonded. Our calculations show that the change in the binding mode of the SCN$^-$ ligands causes a destabilization of the system by ca. 50 kJ mol^{-1}, while there is only a small increase in the strain of the macrocyclic ligand attributted to steric effects caused by the S-bonded SCN$^-$ ligands (Table 3). Thus, electronic effects could also be (at least in part) responsible for the different binding mode of the thiocyanate ligands in **1** and **2**. Further support for this hypothesis comes from a comparison of the N−Pb−N and S−Pb−S angles found in the Cambridge Structural Database[41] for Pb(II) complexes where two thiocyanate ligands coordinate simultaniously to the metal ion. From this search we found N−Pb−N angles of 80.2,[42] 78.2,[43] 81.1,[44] and 113.6°[45] and S−Pb−S angles of 158.0,[46] 158.2,[47] and 180.0°.[48] The experimental N(1S)−Pb(1)−N(2S) angle in **1** amounts 83.4°, while the S(1S)−Pb(1)−S(1S′) angle in **2** is 180° (Table 2). Despite the limited number of examples available in the literature, these results suggest that S-bonded thiocyanate groups are favored when the two ligands occupy trans positions, while N-coordination is more favorable when the two thiocyanate ligands occupy cis positions in the Pb(II) coordination sphere. The electronic reasons behind this effect

(39) Pearson, R. G.; Mawby, R. *J. Halogen Chem.* **1967**, *3*, 55.
(40) Metz, B.; Weiss, R. *Inorg. Chem.* **1974**, *13*, 2094.
(41) Allen, F. H.; Kennard, O. *Chem. Des. Autom. News* **1993**, *8*, 31.
(42) Baranyi, A. D.; Onyszchuk, M.; Fortier, S. *J. Chem. Soc., Dalton Trans.* **1976**, 2301.
(43) Nazarenko, A. Y.; Rusanov, E. B. *J. Coord. Chem.* **1995**, *34*, 265.
(44) Niu, Y.-Y.; Hou, H.-W.; Zhang, Q.-F.; Xin, X.-Q.; Fun, H.-K.; Chautrapromma, S.; Razak, I. A. *Acta Crystallogr., Sect. C* **2001**, *57*, 526.
(45) Harrowfield, J. M.; Miyamae, H.; Skelton, B. W.; Soudi, A. A.; White, A. H. *Aust. J. Chem.* **1996**, *49*, 1067.
(46) Drew, M. G. B.; Rodgers, A.; McCann, M.; Nelson, S. M. *Chem. Commun.* **1978**, 415.
(47) Nazarenko, A. Y.; Rusanov, E. B. *Polyhedron* **1994**, *13*, 2549.
(48) Metz, B.; Eiss, R. *Acta Crystallogr., Sect. B* **1973**, *29*, 1088.

are discussed in the electronic structure calculations described below.

The interconversions between (a)-anti ↔ (b)-anti and (a)-syn ↔ (b)-syn conformations of $\mathbf{L^2}$ complexes were studied in vacuo by using the synchronous transit-guided quasi-Newton method.[22,23] Our results show that the interconversion between (a)- and (b)-conformations is a single-step process involving the rotation of one pendant arm. Both the (a)- and (b)-conformations of syn and anti complexes of $\mathbf{L^2}$ are characterized by dihedral ϕ angles between the aromatic ring plane and that formed by the pivotal nitrogen atom, the carbon atom of the benzyl group, and the aromatic carbon atom attached to it, of ca. 90°. The structures of the transition states that connect the two minimum energy conformations (a) and (b) in both syn and anti complexes present dihedral ϕ angles close to 0°. The in vacuo optimized Cartesian coordinates obtained for both transition state structures are given in the Supporting Information. The computed barriers for the (a) ↔ (b) interconversion process (including NPE terms) amount to 19.15 kJ mol^{-1} (*syn*-[Pb(L^2)($NCS)_2$]) and 16.54 kJ mol^{-1} (*anti*-[Pb(L^2)($SCN)_2$]). These energy barriers are relatively low because the macrocycle pendant arms remain uncoordinated in the complex.

Electronic Structure. To understand the main features of the Pb−ligand bonding in this family of compounds we performed electronic structure calculations on the (a)-*anti*-[Pb(L^2)($SCN)_2$] and (a)-*syn*-[Pb(L^2)($NCS)_2$] systems as model compounds for complexes **1** and **2**. Electronic structure calculations yield the electronic energy and the wave function of a molecular system in a particular electronic state. The wave function itself is not very suitable for interpretation, since it is a function of the coordinates of all electrons. Thus, simplified notions and characteristics of the wave function are needed to get insight into the electronic structure of molecules. The most widely used procedure to obtain information on electronic structure of molecules is the Mulliken population analysis (MPA).[49] The AOMix program takes advantage of the MPA to calculate density-of-states (DOS) and overlap population density-of-states (ODOS) plots.[50] These plots provide pictorial representation of molecular orbital (MO) compositions and their contributions to chemical bonding. The DOS and ODOS plots obtained for the (a)-*anti*-[Pb(L^2)($SCN)_2$] and (a)-*syn*-[Pb(L^2)($NCS)_2$] systems are shown in Figure 6. The DOS spectra were generated from the contributions of three molecular fragments: Pb atom; SCN^- donor atoms; ligand ($\mathbf{L^2}$) donor atoms. A simple inspection of the DOS spectra shown in Figure 6 shows that a given MO has an important contribution from atomic orbitals (AO) of only one of these three fragments. For instance, the main contribution to the highest occupied molecular orbital (HOMO) of both molecules comes from AO of the S or N donor atoms of the SCN^- groups, with a small contribution from AO of Pb and the ligand donor atoms. The main contribution to the lowest unoccupied molecular orbital (LUMO) comes from AO of

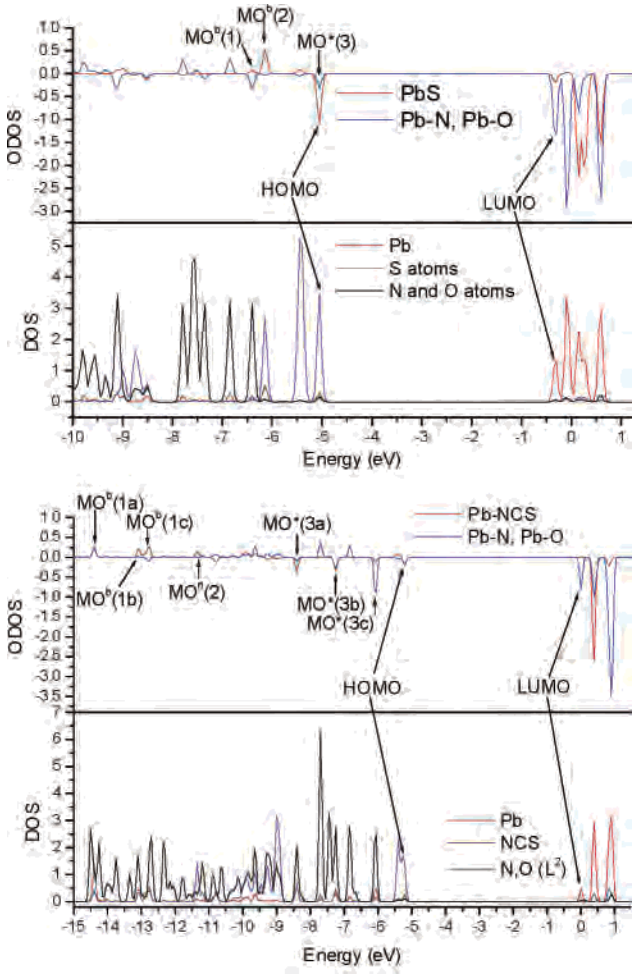

Figure 6. Density-of-states (DOS) and overlap population density-of-states (ODOS) plots of (a)-*anti*-[Pb($\mathbf{L^2}$)($SCN)_2$] (top) and (a)-*syn*-[Pb($\mathbf{L^2}$)($NCS)_2$] (bottom). The DOS spectra show the contributions of three fragments of the molecule: Pb atom, NCS donor atoms; $\mathbf{L^2}$ donor atoms.

the Pb atom, with smaller contributions from AO of the other two fragments. The DOS plots therefore suggest a small degree of covalency of the Pb−ligand bonds. This is in agreement with the electronic populations on the Pb atoms, the net charges calculated by MPA being +1.25 e for (a)-*syn*-[Pb(L^2)($NCS)_2$] and +1.19 e for (a)-*anti*-[Pb(L^2)($SCN)_2$]. The smaller net charge of the latter complex suggest a greater electron density transfer from the NCS^- ligands when they coordinate through the less electronegative S atom. This electron transfer is mainly into the 6p orbitals on the lead atom, as shown by the natural electron configuration calculated for the Pb atom in these complexes: Pb:6s[1.99] 6p[0.73] 7p[0.04] (anti) and Pb:6s[1.94] 6p[0.64] 7p[0.02] (syn), resulting in 6p/6s population ratios of 0.37 (anti) and 0.33 (syn).

The overlap population density-of-states (ODOS) plots obtained for the (a)-*anti*-[Pb(L^2)($SCN)_2$] and (a)-*syn*-[Pb(L^2)($NCS)_2$] systems are shown in Figure 6. These plots provide a pictorial representation of the bonding, nonbonding, or antibonding character of molecular orbitals with respect to particular molecular fragments. A positive value in ODOS plots represents a bonding situation, a negative value represents an antibonding one, and a value close to zero

(49) Mulliken, R. S. *J. Chem. Phys*. **1955**, *23*, 1833.
(50) Ghosh, S.; Gorelsky, S. I.; Chen, P.; Cabrito, I.; Moura, J. J. G.; Moura, I.; Solomon, E. I. *J. Am. Chem. Soc*. **2003**, *125*, 15708.

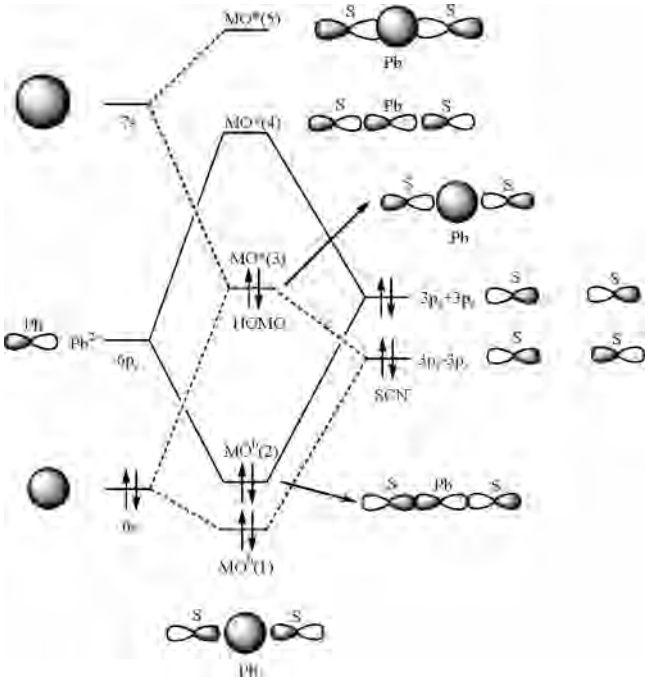

Figure 7. Schematic diagram of the Pb−SCN bond formation in (a)-*anti*-[Pb(**L²**)(SCN)$_2$].

indicates no bonding between the molecular fragments.[50] Figure 6 shows that the HOMO of both syn and anti structures present antibonding character with respect to the Pb−ligand interaction. The Pb−**L²** covalent bond interaction in (a)-*anti*-[Pb(L^2)(SCN)$_2$] is mainly due to the overlap of the unoccupied 6p$_x$ and 6p$_y$ AO orbitals of Pb with the lone pairs of N and O ligand atoms; the strongest Pb−**L²** covalent bonding interaction is the result of the overlap of 2p$_x$ orbitals of the pivotal nitrogen atoms of **L²** with the 6p$_x$ orbital of the Pb atom (MO at −6.85 eV, Figure 6, top). In the case of the (a)-*syn*-[Pb(L^2)(NCS)$_2$] system, the Pb−**L²** covalent bond interaction is also mainly due to the overlap of the unoccupied 6p$_x$ and 6p$_y$ AO orbitals of Pb with the lone pairs of N and O ligand atoms. However, the nature of the covalent bonding interaction between the Pb atom and the thiocyanate ligands in both complexes is rather different. The formation of the Pb−SCN bonds is schematically depicted in Figure 7.

A combination of the two 3p$_z$ orbitals of the S donor atoms overlaps with the 6s and 7s Pb orbitals. As a result, three molecular orbitals are formed labeled as MO^b(1), MO*(3), and MO*(5) (Figure 7). As it can be observed in Figure 6, the MO^b(1) does not contribute much to the Pb−SCN bond formation, probably because the 3p$_z$ AOs of the S atoms are too high in energy compared to the 6s AO of Pb. The MO*(3) has clearly antibonding character with respect to the Pb−SCN interaction and corresponds to the molecular HOMO (see Figures 6 and 7). A combination of the occupied 3p$_z$ orbitals of the S atoms overlaps effectively with the unoccupied 6p$_z$ AO of the Pb atom. As a result, a molecular bonding orbital at −6.14 eV is formed (MO^b(2), Figure 7). This bonding MO presents a large positive value in the ODOS plot (Figure 6), and therefore, represents the most important contribution to the Pb−SCN bond formation.

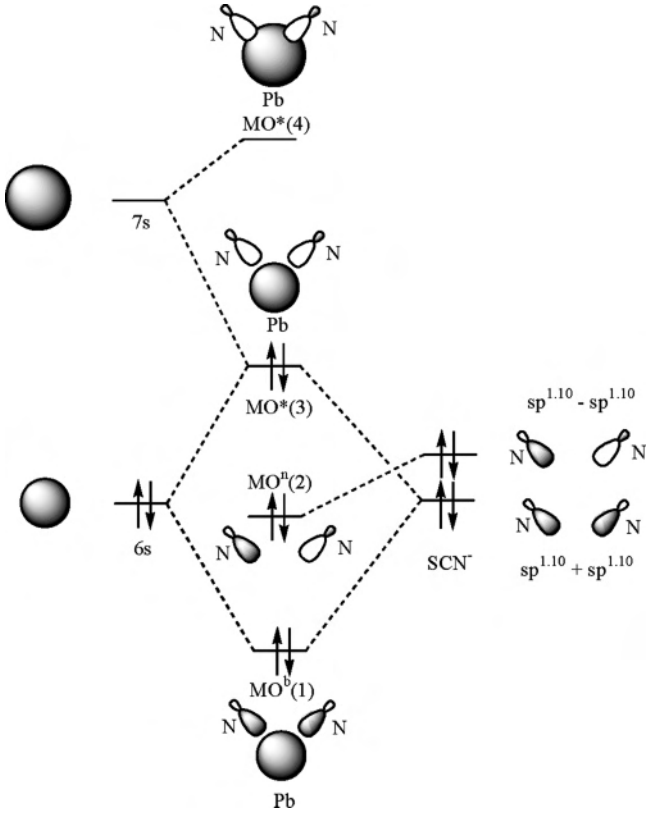

Figure 8. Schematic diagram of the Pb−NCS bond formation in (a)-*syn*-[Pb(**L²**)(NCS)$_2$].

The Pb−NCS bond formation in (a)-*syn*-[Pb(L^2)(NCS)$_2$] is shown schematically in Figure 8. The natural atomic hybrid calculated for the lone pairs of both N atoms of the NCS$^-$ ligands by NBO analysis is sp$^{1.10}$. The Pb−NCS covalent bonding interaction is primarly due to the overlap of the 6s and 7s AO of Pb with a combination of these sp$^{1.10}$ hybrids (Figure 8), which leads to the formation of MO^b(1). As shown in Figure 8, two antibonding orbitals are formed as byproducts of the Pb−NCS bond formation (MO*(3) and MO*(4)). The 6p AO of Pb does not contribute significantly to the Pb−NCS bond formation. As a result, a primarily nonbonding MO with a contribution of sp AO of the N atoms is formed (MO^n(2), Figure 8). In practice, this rather simplified view is complicated because both MO^b(1) and MO*(3) are heavily mixed with the N and O lone pairs of the **L²** ligand. As a consequence, the MO^b(1) orbital shown in Figure 8 splits into three molecular orbitals labeled as MO^b(1a), MO^b(1b), and MO^b(1c) (Figure 6). As it can be observed in Figure 6, these molecular orbitals present bonding [MO^b(1a)], nonbonding [MO^b(1b)], and antibonding [MO^b(1c)] character with respect to the Pb−**L²** interaction. Similary, three molecular orbitals (MO*(3a), MO*(3b), and MO*(3c)) with increasing antibonding character with respect to the Pb−**L²** interaction are formed by combination of MO*(3) and the N and O lone pairs of the **L²** ligand.

As discussed above, the solid-state structures reported in the literature of Pb(II) complexes where two thiocyanate ligands are simultaneously coordinated to the metal ion suggest that two S-bonded thiocyanate groups are favored when the resultant S−Pb−S angle is close to 180°, while

the presence of two N-bonded thiocyanate groups is characterized by N−Pb−N angles of ca. 80°. These experimental results can be rationalized on the basis of our DFT calculations reported here. As depicted in Figure 7, the Pb−SCN bond formation occurs mainly through the overlapping of the occupied $3p_z$ orbitals of the S atoms with the unoccupied $6p_z$ AO of the Pb atom, while the $3p_z$ AOs of the S atoms are too high in energy compared to the 6s AO of Pb. As a consequence, the simultaneous formation of two Pb−SCN bonds is more favorable for S−Pb−S angles close to 180°, for which the overlap between the occupied $3p_z$ orbitals of the S atoms and the unoccupied $6p_z$ AO of the Pb atom is maximized. On the contrary, the Pb−NCS covalent bonding interaction is primarily due to the overlap of the 6s AO of Pb with $sp^{1.10}$ hybrids of the thiocyanate groups. The 6s AO of Pb has spherical symmetry, and therefore, one would expect N−Pb−N angles different from 180° to occur. Thus, our electronic structure calculations can rationalize the different coordination of the thiocyanate groups in compounds **1** and **2**.

Shimoni-Livny et al.[36] investigated a close relation between the role of a lone pair of Pb(II) and coordination geometry for a number of Pb(II) complexes. They found two general structural categories of Pb(II) compounds: holodirected and hemidirected. These are distinguished by the disposition of ligands around the metal ion. In the hemidirected form there is a void in the liganding which is not found with holodirected geometry. According to their calculations, the lone pair orbital in hemidirected complexes has p character and thus the ligands tend to bond to the Pb atom away from the lone pair. An analysis of the natural bond orbitals (NBOs) in (a)-*anti*-$[Pb(L^2)(SCN)_2]$ shows that the Pb(II) lone pair orbital remains almost entirely s in character: s[99.99%]p0.00[0.01%]. This indicates that the $6s^2$ lone pair remains inactive, as expected for compounds with a holodirected ligand distribution.[36,51,52] The analysis of the NBOs in (a)-*syn*-$[Pb(L^2)(NCS)_2]$ shows that the Pb(II) lone pair orbital is still predominantly 6s but slightly polarized by a small 6p contribution: s[98.37%]p0.02[1.63%]. However, this small p contribution does not result in the void in the distribution of ligands characteristic of hemidirected complexes.

(51) Hancock, R. D.; Shaikjee, M. S.; Dobson, S. M.; Boeyens, J. C. A. *Inorg. Chim. Acta* **1988**, *154*, 229.
(52) Hancock, R. D. In *Perspectives in Coordination Chemistry*; Williams, A. F., Floriani, C., Merbach, A. E., Eds.; VHCA: Basel, Switzerland, 1992.

Conclusions

The X-ray crystal structures of $[Pb(L^2)(NCS)_2]$ (**1**) and $[Pb(L^4)(SCN)_2]$ (**2**) show very different conformations of the macrocyclic receptors despite their very similar coordinative properties: the organic receptor adopts a syn conformation in **1**, while the lariat ether in **2** shows an anti conformation. The coordination of the SCN^- groups is also different in both complexes. While in compound **1** coordination occurs through the N atoms, in **2** the thiocyanate groups are S-bonded. A DFT study performed in vacuo predicts the syn conformation being the most stable for both the $\mathbf{L^2}$ and $\mathbf{L^4}$ complexes. Electronic structure calculations evidence a high electrostatic character of the Pb−ligand bonds in these holodirected complexes. They also suggest a greater transfer of electron density from the NCS^- ligands when they coordinate through the less electronegative S atom. Our DFT calculations reveal a different nature of the Pb−SCN and Pb−NCS bond formation. The Pb−SCN bond formation occurs mainly due to an effective overlap of the occupied $3p_z$ orbitals of the S atoms and the unoccupied $6p_z$ AO of the Pb atom, while the Pb−NCS bonding interaction is primarily due to the overlap of the 6s and 7s AO of Pb with $sp^{1.10}$ hybrids of the N donor atoms. Thus, our electronic structure calculations can rationalize the different coordination of the thiocyanate groups in compounds **1** and **2**: the simultaneous formation of two Pb−SCN bonds is more favorable for S−Pb−S angles close to 180°, for which the overlap between the occupied $3p_z$ orbitals of the S atoms and the unoccupied $6p_z$ AO of the Pb atom is maximized. This work demonstrates that our computational approach provides accurate molecular geometries for relatively complicated lead(II) complexes. The calculated conformational energies are also in qualitative agreement with the experimental findings. Finally, electronic structure calculations allow one to rationalize the chemical bonding in these family of compounds.

Acknowledgment. The authors thank the Xunta de Galicia (Grant PGIDIT03TAM10301PR) for generous financial support. The authors are also indebted to the Centro de Supercomputación of Galicia (CESGA) for providing the computer facilities.

Supporting Information Available: X-ray crystallographic files in CIF format for **1** and **2** and in vacuo optimized Cartesian coordinates (Å) of energy minima and saddle points of the $\mathbf{L^2}$ and $\mathbf{L^4}$ complexes. This material is available free of charge via the Internet at http://pubs.acs.org.

IC048768Y